Small Molecule Therapeutics

Efficacy of the MDM2 Inhibitor SAR405838 in Glioblastoma Is Limited by Poor Distribution Across the Blood–Brain Barrier

Minjee Kim[1], Daniel J. Ma[2], David Calligaris[3,4], Shuangling Zhang[1], Ryan W. Feathers[5], Rachael A. Vaubel[2], Isabelle Meaux[6], Ann C. Mladek[2], Karen E. Parrish[1], Fang Jin[2], Cedric Barriere[6], Laurent Debussche[6], James Watters[6], Shulan Tian[2], Paul A Decker[2], Jeanette E. Eckel-Passow[2], Gaspar J. Kitange[2], Aaron J. Johnson[2], Ian F. Parney[2], Panos Z. Anastasiadis[5], Nathalie Y.R. Agar[3,4,7], William F. Elmquist[1], and Jann N. Sarkaria[2]

Abstract

Controversy exists surrounding whether heterogeneous disruption of the blood–brain barrier (BBB), as seen in glioblastoma (GBM), leads to adequate drug delivery sufficient for efficacy in GBM. This question is especially important when using potent, targeted agents that have a poor penetration across an intact BBB. Efficacy of the murine double minute-2 (MDM2) inhibitor SAR405838 was tested in patient-derived xenograft (PDX) models of GBM. *In vitro* efficacy of SAR405838 was evaluated in PDX models with varying MDM2 expression and those with high (GBM108) and low (GBM102) expression were evaluated for flank and orthotopic efficacy. BBB permeability, evaluated using TexasRed-3 kDa dextran, was significantly increased in GBM108 through VEGFA overexpression. Drug delivery, MRI, and orthotopic survival were compared between BBB-intact (GBM108-vector) and BBB-disrupted (GBM108-VEGFA) models. MDM2-amplified PDX lines with high MDM2 expression were sensitive to SAR405838 in comparison with MDM2 control lines in both *in vitro* and heterotopic models. In contrast with profound efficacy observed in flank xenografts, SAR405838 was ineffective in orthotopic tumors. Although both GBM108-vector and GBM108-VEGFA readily imaged on MRI following gadolinium contrast administration, GBM108-VEGFA tumors had a significantly enhanced drug and gadolinium accumulation, as determined by MALDI-MSI. Enhanced drug delivery in GBM108-VEGFA translated into a marked improvement in orthotopic efficacy. This study clearly shows that limited drug distribution across a partially intact BBB may limit the efficacy of targeted agents in GBM. Brain penetration of targeted agents is a critical consideration in any precision medicine strategy for GBM.

Mol Cancer Ther; 17(9); 1893–901. ©2018 AACR.

Introduction

Individualized medicine approaches based on next-generation sequencing (NGS) could significantly improve the dismal outcome for the most common and aggressive primary brain tumor, glioblastoma (GBM; ref. 1). However, the majority of targeted agents exhibit limited partitioning into the brain, which could limit efficacy, especially given the invasive nature of GBM (2–6). Although essentially all GBM exhibit some accumulation of radiographic contrast on clinical imaging, whether contrast enhancement translates into meaningful drug accumulation remains uncertain (7). Furthermore, image-guided surgical biopsy studies also demonstrate that most patients have significant tumor burden outside of contrast-enhancing regions (8). Therefore, the focus of this study was to evaluate the influence of blood–brain barrier (BBB) integrity on the efficacy of a molecularly-targeted agent with limited brain penetration.

Disruption of the p53 tumor-suppressor pathway occurs in the majority of GBM and is driven by amplification of the *murine double minute 2* (*MDM2*) locus in approximately 14% of patients (9). MDM2 is known to be a major regulator of p53, by targeting p53 for degradation mainly through its intrinsic E3 ubiquitin ligase. As a result, high MDM2 expression can effectively suppress p53 expression and activity (10). Reactivation of p53 can be achieved through diverse pharmacologic strategies, including: suppression of MDM2 expression, inhibition of E3 ubiquitin ligase activity, or inhibition of the p53-MDM2-proteasome interaction, with the latter approach favored by the current generation of MDM2 inhibitors (11–13). Among small-molecule MDM2 inhibitors, SAR405838 is clinically advanced in that it is in phase one clinical trials. SAR405838 has a high MDM2 selectivity based on a fluorescence binding assay, with a K_i of 0.88 nmol/L, and evidence of antitumor activity in a variety of tumor types (14). The studies reported herein were designed to assess the potential use of SAR405838 in *MDM2-*

[1]University of Minnesota, Minneapolis, Minnesota. [2]Mayo Clinic, Rochester, Minnesota. [3]Brigham and Women's Hospital, Boston, Massachusetts. [4]Harvard Medical School, Boston, Massachusetts. [5]Mayo Clinic, Jacksonville, Florida. [6]Sanofi Oncology, Vitry-sur-Seine, France. [7]Dana Farber Cancer Institute, Boston, Massachusetts.

Note: Supplementary data for this article are available at Molecular Cancer Therapeutics Online (http://mct.aacrjournals.org/).

M. Kim and D.J. Ma contributed equally to this article.

Corresponding Author: Jann N. Sarkaria, 200 First Street, SW, Rochester, MN 55905. Phone: 507-284-9025; Fax: 507-284-3906; E-mail: Sarkaria.jann@mayo.edu

doi: 10.1158/1535-7163.MCT-17-0600

AACR **1893**

amplified GBM to further the clinical development of a precision medicine strategy.

The objective of this study was to examine possible reasons for the lack of efficacy in orthotopic GBM models of an otherwise active compound, the MDM2 inhibitor SAR405838. We used a PDX GBM model that overexpressed MDM2, and investigated the role of drug delivery across the BBB as a reason for lack of efficacy. Manipulations of the permeability of the BBB, through VEGFA expression, were tested. The results clearly indicate that the BBB was a limiting factor in drug delivery and subsequent efficacy.

Materials and Methods

Cell culture, drugs, and apoptosis

Short-term explant cultures were obtained from a primary, patient derived glioblastoma panel and were grown in neurobasal media (Life Technologies) as previously described (15, 16). Cell authentication was performed using STR profiling last performed on 4/5/2015. Neurosphere formation and Cyquant proliferation assays were performed as previously described (15). SAR405838 was obtained from Sanofi (Vitry-sur-Seine, France). Annexin-V assays were performed as previously described (17).

TP53 gene Sequencing

Purified genomic DNA (50 ng) was PCR amplified in a 25 µL PCR reaction using primers that were designed to flank exons 4-8 of TP53 gene. Primer sequences are available in Supplementary Materials. The products were then submitted to Mayo Clinic Sequencing facility for Sanger sequencing. Mutations were detected using Mutation Surveyor software V4.0.9 (Softgenetics).

MDM2 amplification and RNA expression

RNA was extracted from 20 mg of frozen flank tumor using the Qiagen Puregene Core Kit A (Cat# 158667) and the Qiagen RNeasy Mini Kit (Cat# 74106), then quantitated on a Nanodrop 2000. Three tumor samples were used per GBM line.

Real-time PCR assays

Total RNA was extracted with the RNeasy kit (Qiagen) according to the manufacturer's instructions and cDNA was synthesized using the High Capacity cDNA Reverse Transcription kit (Applied Biosystems). TaqMan gene-expression assays were performed by using MDM2 (Hs99999008-m1), p21 (Hs00355782-m1), PUMA (Hs00248075) gene-specific primer/probe sets (Applied Biosystems) for real-time PCR amplification in an Applied Biosystems 7900 thermocycler. RPL37a was used for normalization using probes and primers from Applied Biosystems. Relative quantification of mRNA was calculated by comparative cycle threshold ($\Delta\Delta C_t$) method.

Efficacy studies in vivo

All animal studies were approved by the Mayo Institutional Animal Care and Use Committee. Subcutaneous xenografts were established by injecting the flank of athymic nude mice with 1×10^6 cells suspended in Matrigel/PBS. When established tumors reached 150 to 250 mm^3 in size, mice were randomized and treated by oral gavage with placebo vehicle (98% PEG200: 2% TPGS) or SAR405838 (50 mg/kg/d). Tumor volume was measured thrice weekly until euthanasia. To prepare cells for orthotopic models, flank tumor xenografts were harvested, mechanically disaggregated, and grown in short-term cell culture (5–14

days) in DMEM supplemented with 2.5% FBS, 1% penicillin, and 1% streptomycin. Cells were harvested by trypsinization and injected (3×10^5 or 1×10^6 cells per mouse, suspended in 10 µL) into the right basal ganglia of anesthetized athymic nude mice (athymic Ncr-nu/nu, National Cancer Institute) using a small animal stereotactic frame (ASI Instruments) as previously described (18). Mice were randomized and treated with either placebo vehicle or 50 mg/kg of SAR405838 per day as described above on day 29 after the tumor injection. Mice were observed daily and euthanized upon reaching a moribund state. For pharmacodynamic assessment, tumors were harvested at 24 hours after the last drug dose.

Brain-to-plasma ratio for SAR405838

In vivo brain-to-plasma ratios were determined in Friend leukemia virus strain B (FVB) wild-type mice of either sex from an FVB genetic background (Taconic Farms). Five mice in each genotype were orally dosed with 25 mg/kg SAR405838 using the same vehicle as was used in the efficacy studies. Animals were euthanized using a CO_2 chamber 1 hour after dosing. Blood was collected by cardiac puncture in heparinized tubes and plasma were separated after centrifugation at 3,500 rpm for 15 minutes at 4°C. Whole brain was harvested at the same time as the blood collection. Samples were analyzed by a Micromass Quattro Ultima mass spectrometer coupled with AQUITY UPLC system (Waters) to measure the concentration of SAR405838 in plasma and brain samples. PLX4720 was used as an internal standard. Isocratic elution was used with 45% of acetonitrile as an organic phase and 55% of water with 0.1% formic acid. Total run time was 8 minutes, and the flow rate was 0.5 mL/min. Retention time were 1.95 minutes for SAR405838 and 5.45 minutes for the internal standard. Mass-to-charge ratio (m/z) transition was 560 > 305.9 for SAR405838 and 411.9 > 304.86 for the internal standard. The assay was validated and was precise and linear to determine concentrations in the range observed *in vivo*.

VEGFA overexpression

GBM108 cells were transduced with either an empty vector (LV197, Genecopoeia Inc., Cat# EX-NEG-Lv197) or a vector containing VEGFA transcript variant 4 (NM_001171626.1, Cat# EX-Z0781-Lv197) as previously described (19).

VEGFA ELISA

Cell lysates from GBM108 parental, GBM108 empty vector, and GBM108 VEGFA transfected cells were harvested with 1% Triton X in DPBS (Hyclone, GE Life Sciences) after rinsing with ice cold DPBS. Total cell protein was quantified by the Pierce BCA protein assay kit (Thermo Scientific). A human VEGF Quantikine ELISA kit (R&D Systems) was used to quantify VEGFA expression in the culture supernatant. Levels of VEGFA expression were normalized to total cell protein in corresponding wells. The three lines were compared using one-way ANOVA followed by Bonferroni's test for multiple comparisons.

TUNEL Staining

Apoptosis was analyzed by using an ApopTag Plus peroxidase in situ apoptosis detection kit (S7101, Millipore). GBM108 cells were injected to the mouse flank ($n = 10$). Mice were randomized into 2 groups of 5 mice when the tumor reached 250 to 400 mm^3. The placebo group was dosed daily with vehicle, and treatment group was dosed daily with SAR405838, 50 mg/kg, for 5 days.

Tumors were harvested on the fifth day 2 hours after last dose of drug and flash frozen. Tumors were formalin-fixed, paraffin embedded, and sliced at a thickness of 5 μm for staining. Bright field images were acquired using a Leica DMI6000B inverted microscope at ×40. Six images were taken for each tumor and apoptotic cells/bodies were counted blinded with respect to the treatment groups.

Texas red imaging to evaluate BBB integrity

Tumor-bearing mice were injected with 3 kD dextran conjugated with Texas Red (Molecular Probes, Thermo Fisher Scientific) in the tail vein 10 minutes before CO_2 euthanasia. Whole brain was harvested after cardiac perfusion with room temperature 4% PFA in saline. The brain was frozen on dry ice and stored at −80°C. Cryostat sections of 20 μm were obtained at −21°C (Leica 3050S), mounted on glass slides and stored at −20°C before imaging. Whole brain slices were imaged using a Nikon AZ100M macroscope at ×16 and Nikon software compiled individual images. All slides were imaged on the same day using 400 ms exposure and cresyl violet staining was done to locate the tumor for comparison.

Preclinical MRI acquisition and analysis

MRI was performed using a Bruker DRX-300 (300 MHz 1H) 7 Tesla vertical-bore small animal imaging system (Bruker Biospin) according to published protocols (20, 21). Throughout imaging, mice were anesthetized by inhalation of 3% to 4% isofluorane in air and their respiratory rate monitored. For T1 weighted imaging, mice were administered gadolinium contrast (Gadavist 1 mmol/L, Bayer) intraperitoneally at a dose of 100 mg/kg and imaged after a 15 minute delay.

MALDI MSI

Mass spectra of mouse brain tissue sections were acquired using a SolariX XR Fourier transform ion cyclotron resonance mass spectrometer (FT-ICR; 12 T; Bruker Daltonics). MALDI MSI experiments were acquired with a pixel step size for the surface raster set to 80 μm in FlexImaging 4.0 software (Bruker Daltonics). The analyses were performed in positive ion mode by continuous accumulation of selected ions (CASI) in a mass range comprised between m/z 440–620 and a laser intensity set to 40%. Each mass spectrum is the sum of 250 laser shots randomized over 10 positions within the same spot (25 shots/position) at a laser frequency of 1,000 Hz. The MALDI images were displayed using FlexImaging 4.0. The permeability of SAR405838 through the blood vessel was visualized following the signal of the drug (m/z 562.2034 ± 0.001) and a biomarker of vasculature (heme at m/z 616.1768 ± 0.001), as previously described (22). Gadavist was visualized following the signal of one of the isotopologue peaks of the contrast agent at m/z 606.1409 ± 0.001.

Immunohistochemistry and quantitative analysis

Staining for human p21 was performed using a rabbit monoclonal antibody 12D1 (Cell Signaling Technology) followed by hematoxylin counterstaining. p21 positivity was determined by adapting the Aperio IHC Nuclear Image Analysis algorithm, which uses color de-convolution to separate the DAB (positive) from hematoxylin (negative) signals, to the nuclei staining patterns and shapes present in these samples. The percentage of all stained nuclei that were positive for the DAB chromogen as a marker of p21 was quantitated.

Statistical analyses

In vitro data presented are the mean ± SE from three or more experiments. Two-tailed Student *t* tests and one-way ANOVA were used to measure statistical differences. *P* values <0.05 were considered statistically significant. Statistical analysis of animal survival and tumor progression was performed using the log-rank test.

Results

In vitro efficacy of SAR405838

The Mayo Clinic has developed a large panel of GBM patient-derived xenograft (PDX) models, and to identify the most relevant models for studying an MDM2 inhibitor, a series of studies were used to select models for further analysis. Initially, 55 PDX models were evaluated for *MDM2* transcript expression by qRT-PCR (Supplementary Fig. S1), and then 5 lines, including high and low expressing lines, were selected for whole exome sequencing to determine MDM2 amplification and copy status (Supplementary Fig. S2). These selected lines were further evaluated for p53 mutation status by Sanger sequencing. The dose response curves for SAR405838 in these tumor lines were obtained by *in vitro* neurosphere formation and CyQuant assay to determine potency (Fig. 1A). SAR405838 had the best potency in GBM108. Treatment with 100 nmol/L SAR405838 significantly reduced neurosphere formation in all 4 wild-type p53 tumor lines, but the reduction in neurosphere formation was significantly more profound in the MDM2 amplified/over-expressing GBM108 (5.8 ± 1.2% relative to control) and GBM143 (6.4 ± 6.1%) lines as compared with GBM10 (44.6 ± 6.2%) and GBM102 (33.6 ± 17.1%) lines without MDM2 transcript over-expression (Fig. 1B). In an evaluation of apoptosis induction, SAR405838 treatment was associated with a significantly increased fraction of Annexin V-positive cells, relative to control, only in GBM108 (41.5 ± 9.4% vs 9.4 ± 2.3% *P* < 0.0001) and GBM143 (23.9 ± 9.8% vs 9.8 ± 2.0% *P* = 0.003) cells (Fig. 1C). Consistent with robust disruption of MDM2 activity, 24-hour exposure to 100 nmol/L SAR405838 resulted in marked induction of p53 transcriptional targets PUMA and p21 (Fig. 1D). In conjunction with previously published studies, these data support a model in which SAR405838 achieves cytotoxicity in MDM2 over-expressing tumors through restored p53 function and subsequent apoptosis (23).

In vivo efficacy of SAR405838

The efficacy of SAR405838 was evaluated in a series of flank and intra-cranial *in vivo* studies. Consistent with the *in vitro* results, SAR405838 induced tumor regression and uniformly suppressed growth of GBM108 flank tumors for over 6 weeks of therapy (50 mg/kg p.o. qd until euthanasia, Fig. 2A), whereas drug treatment was ineffective in GBM102 flank tumors (Fig. 2B). This regimen was well-tolerated for the entire treatment course. The average weight of the mice at the end of treatment was 106% ± 4% of the beginning weight. In the sensitive GBM108 model, SAR405838 treatment for 5 days resulted in a 21-fold increase in p21 transcript expression and a 7-fold increase in PUMA expression 24 hours after drug treatment (Fig. 2C). As a result, SAR405838 treatment increases apoptosis in the GBM108 model by 3-fold relative to placebo treatment, as measured by TUNEL-positivity (Supplementary Fig. S3). In contrast with the profound efficacy observed in flank models, the same SAR405838 dosing
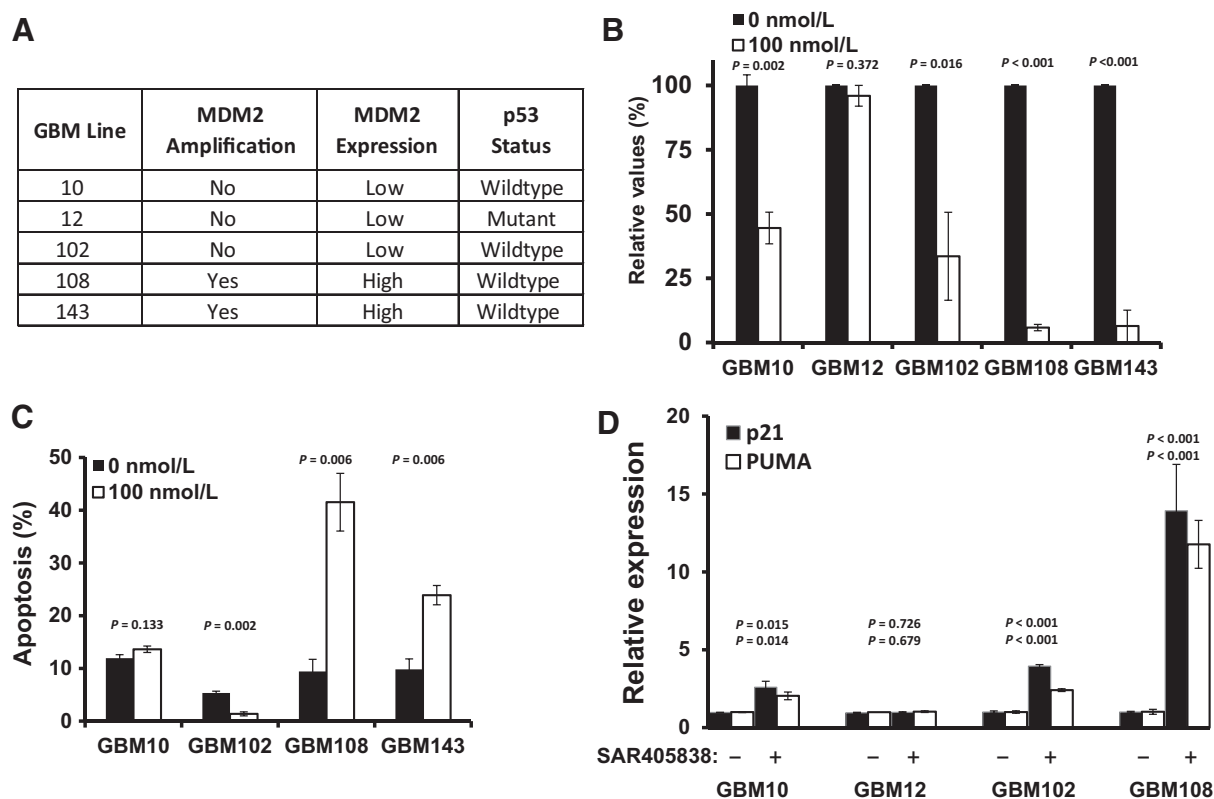
Figure 1.
Characteristics of selected PDX GBM lines. **A,** Summary of MDM2 amplification, expression, and p53 status for select xenograft lines. **B,** Relative values of tumor growth with the treatment of SAR405838 (100 nmol/L) compared with controls are measured either neurosphere formation or CyQuant (CyQuant measurement for GBM108). SAR405838 (100 nmol/L) has higher inhibition in MDM2 overexpressed, p53 WT lines (GBM108, GBM143) when compared with MDM2-low lines (GBM10, 12, 102). **C,** SAR405838 (0 nmol/L black, 100 nmol/L gray) induces more apoptosis by Annexin V at 72 hours in MDM2 overexpressed lines (GBM108, GBM143) when compared with MDM2-low lines (GBM10 and GBM102). **D,** Relative transcript expression of p21 and PUMA. Short-term explant cultures were treated with vehicle or 100 nmol/L SAR405838 and then processed for qRT-PCR. Results represent the mean ± SE with P values for p21 (top) and PUMA (bottom). *, $P < 0.05$; **, $P < 0.01$; ***, $P < 0.001$.

regimen was completely ineffective in GBM108 grown as orthotopic tumors (Fig. 2D), which were established at the same time as the GBM108 flank study.

Drug delivery to orthotopic tumors might be limited by a partially intact BBB, and consistent with this concept, limited intratumoral accumulation of a BBB-impenetrant Texas Red-3 kD dextran conjugate was observed in orthotopic GBM108 tumors (Supplementary Fig. S4). Moreover, measurement of SAR405838 drug distribution into the brain demonstrated the brain-to-plasma ratio for SAR405838 was 0.01 ± 0.003 post 1 hour after single oral dosing in non-tumor bearing mice. Overall, these data suggest that restricted partitioning across a partially intact BBB in orthotopic tumors might limit SAR405838 efficacy in an otherwise highly responsive tumor model.

Imaging of BBB integrity

The influence of limited drug delivery across the BBB on treatment efficacy was tested by manipulating the integrity of the tumoral BBB. VEGFA is a pro-angiogenic cytokine that drives the development of an immature, leaky vasculature within GBM, and previous studies have used exogenous delivery of VEGFA to disrupt the BBB (24–26). Therefore, we used a lentiviral expres-

sion system to overexpress VEGFA in GBM108 (GBM108-VEGFA; Supplementary Fig. S5). Importantly, VEGFA over-expression did not meaningfully change the *in vitro* SAR405838 sensitivity of GBM108-VEGFA cells as compared with empty vector transduced GBM108-Vector cells (Supplementary Fig. S6). Using these two GBM108 sub-lines, the impact of VEGFA over-expression on BBB integrity was evaluated by injecting mice 10 minutes before euthanasia with a TexasRed-3 kD dextran conjugate that only accumulates in brain regions with a physically disrupted BBB. Following sectioning and subsequent processing for fluorescence microscopy, this allows a visual evaluation of BBB integrity that is inversely related to red fluorescent intensity. Consistent with limited disruption of the BBB in the parental PDX model (Supplementary Fig. S4), faint and heterogeneous red fluorescence is apparent in GBM108-Vector orthotopic tumors (Fig. 3A). In contrast, the BBB within GBM108-VEGFA tumors was markedly disrupted with brighter and homogeneous red fluorescence across the intra-cranial tumors (Fig. 3A). MRI also provides a sensitive measure of BBB deregulation in brain tumors. Even minimal disruptions of the BBB can result in increased fluid accumulation within tissues that can be readily detected on T2-weighted image sequences, and T1-weighted imaging sequences are highly sensitive for detecting accumulation of paramagnetic gadolinium
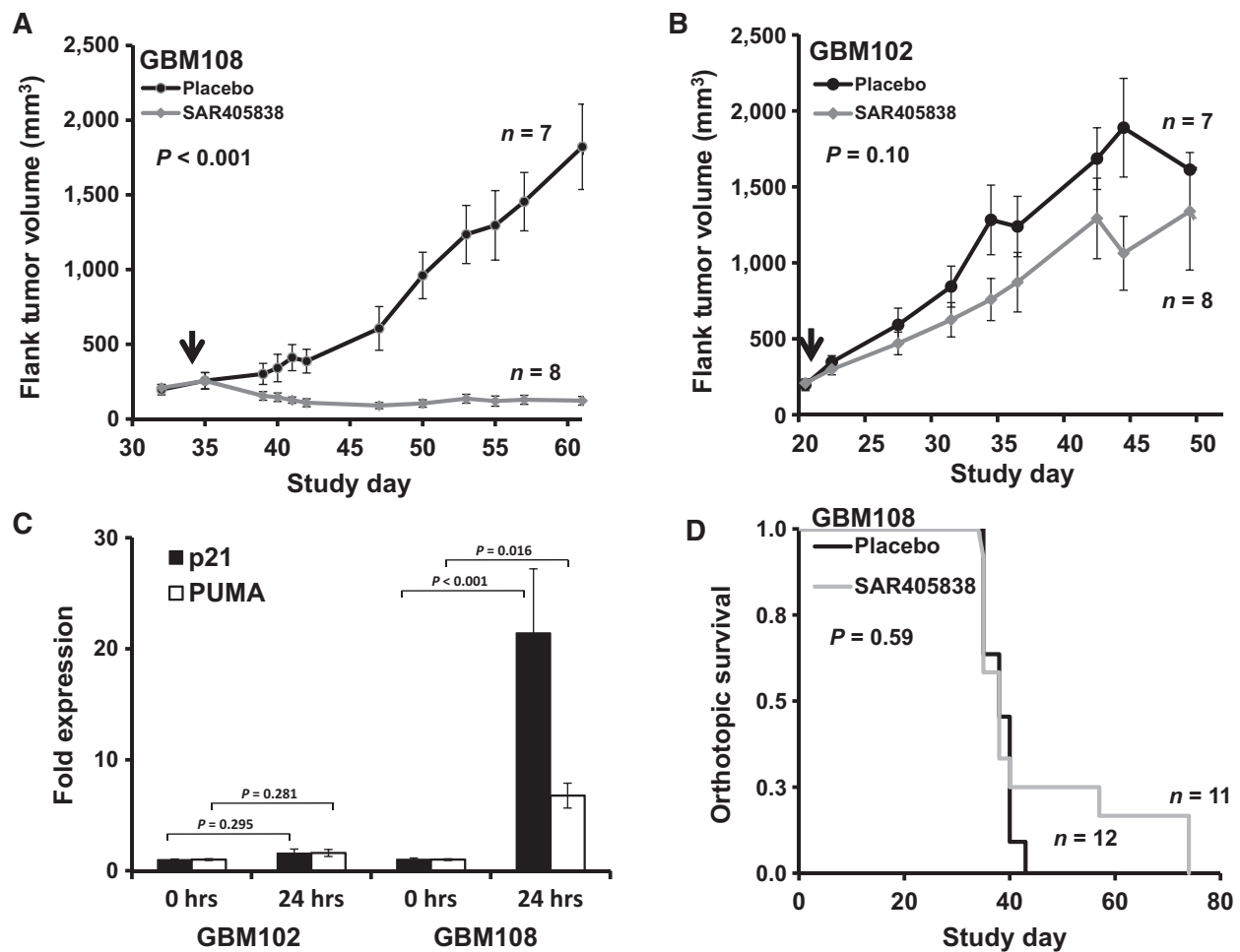
Figure 2.

In vivo efficacy of SAR405838 in heterotopic and orthotopic models of GBM108. **A** and **B,** Average flank tumor volume of surviving mice in placebo (black, $n = 7$) versus SAR405838 at 50 mg/kg p.o. qd until euthanasia (gray, $n = 8$). Solid arrows at treatment start date. Mice were euthanized once tumor exceeded 1800 mm^3. **C,** *In vivo* (flank) expression of p21 and PUMA is increased at 24 hours after SAR405838 (50 mg/kg) in GBM108 but not GBM102. **D,** SAR405838 at the same dosing regimen does not demonstrate efficacy in an orthotopic model of GBM108. [Placebo: black ($n = 12$), Treated: gray ($n = 11$)].

contrast agents, which do not cross an intact BBB. In this context, mice with orthotopic tumors with either GBM108 sub-lines were subjected to MR imaging (Fig. 3B). Consistent with clinical imaging of GBM, orthotopic GBM108-Vector tumors were evident on T2- and T1-post contrast MR images, and consistent with greater disruption of the BBB, the tumor-associated T2- and T1-signals were more evident in the GBM108-VEGFA tumors. Collectively, these data demonstrate that GBM108 tumors have a partially intact BBB that is markedly more disrupted in association with VEGFA overexpression.

The marked disruption of the BBB in GBM108-VEGFA, as compared with the isogenic GBM108-Vector model, provides a platform for evaluating the potential impact of the BBB on imaging, drug delivery, and efficacy in GBM. Accordingly, gadolinium-based contrast (Gadavist) and SAR405838 distribution into orthotopic tumors were evaluated using matrix-assisted laser desorption/ionization mass spectrometric imaging (MALDI MSI; Fig. 3C). Mice with established GBM108-VEGFA ($n = 3$) or GBM108-Vector ($n = 3$) orthotopic tumors

were euthanized after a single Gadavist and SAR405838 dose and processed for histologic sectioning and MALDI MSI. As suggested by T1-post contrast imaging, both GBM108-Vector and GBM108-VEGFA demonstrated intratumoral Gadavist distribution on MALDI MSI with Gadavist distribution in GBM108-VEGFA being appreciably higher. Consistent with the limited efficacy of SAR405838 in parental GBM108 orthotopic tumors, SAR405838 accumulation within GBM108-Vector was relatively low and highly heterogeneous (Fig. 3C; Supplementary Fig. S7). In contrast, accumulation of SAR405838 in orthotopic GBM108-VEGFA was much higher and more homogeneous throughout the tumor.

Effect of SAR405838 brain penetration on efficacy

Effective suppression of MDM2-p53 interaction should promote p53 signaling, and consistent with this expected pharmacodynamic effect on the p53 transcriptional target p21, daily SAR405838 dosing for 4 days in orthotopic GBM108-VEGFA resulted in an 11.3-fold increase in the fraction of p21-positve
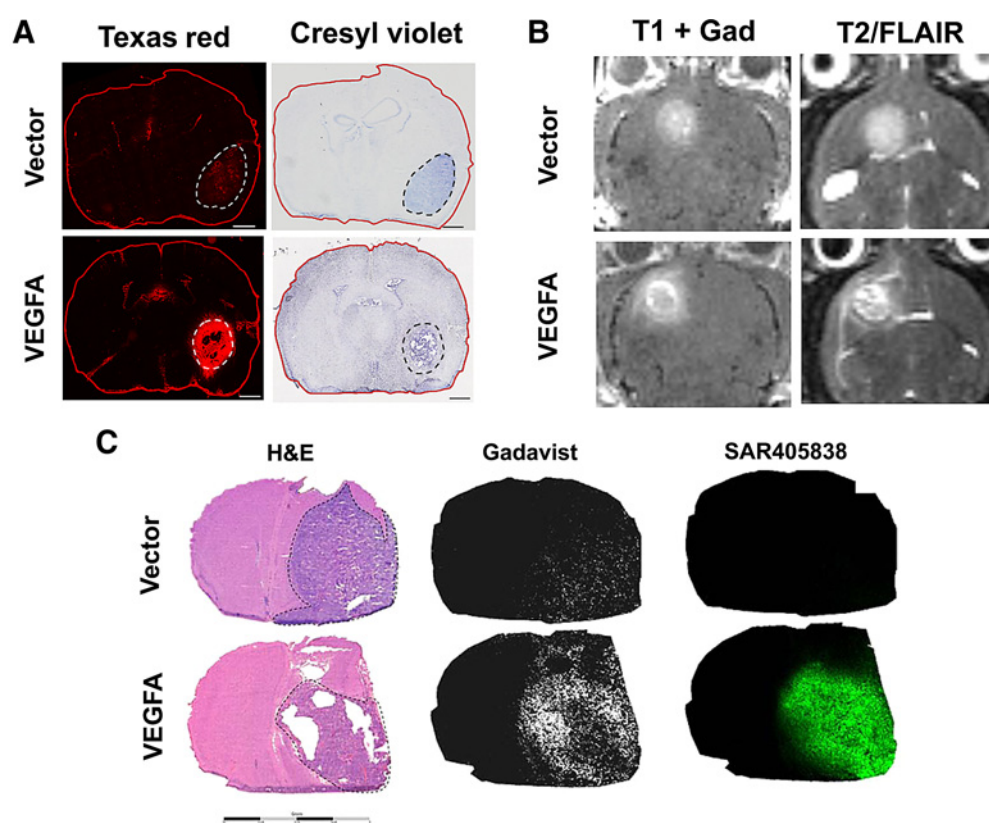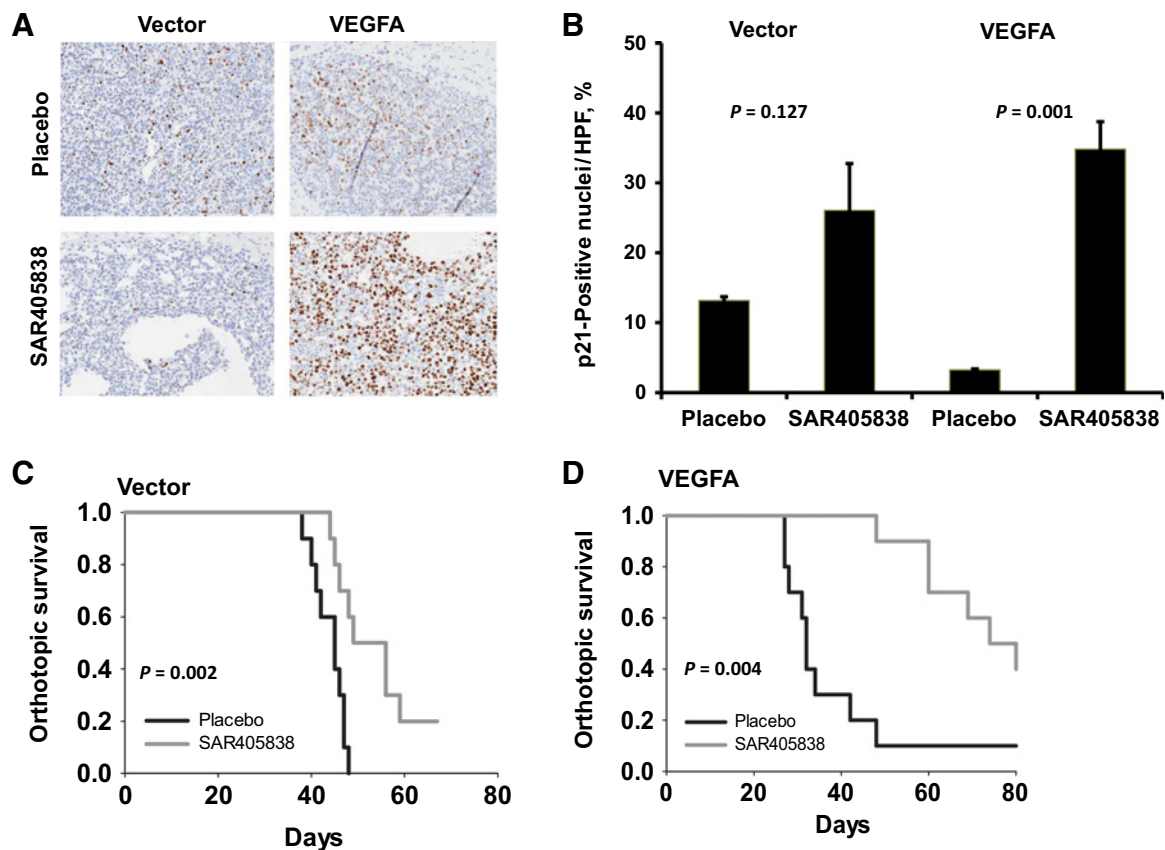
Figure 3.
BBB permeability and distribution of SAR405838 in GBM108-Vector and GBM108-VEGFA. **A,** Comparison of BBB permeability with Texas Red Dextran in GBM108-Vector and GBM108-VEGFA (scale bar, 1,000 μm). **B,** Contrast enhancement on MRI for GBM108-Vector and GBM108-VEGFA. **C,** Comparison of H&E staining in GBM108-Vector and GBM108-VEGFA with MALDI mass spectrometry imaging for Gadavist and SAR405838. Dotted lines on the H&E-stained section images delineate GBM108-Vector and GBM108-VEGFA tumors.

nuclei (Fig. 4A, p21-positive nuclei: 3.2% ± 0.2% with placebo versus 34.8% ± 3.9% with SAR405838 treatment; $P = 0.0002$). In comparison, SAR405838 dosing in orthotopic GBM108-Vector only resulted in a 2-fold increase in p21 staining (Fig. 4B, 13.2% ± 0.6% vs. 26.1% ± 6.7%; $P = 0.006$, respectively). Finally, the influence of enhanced drug delivery on treatment efficacy was evaluated in both GBM108 sub-lines. SAR405838 treatment had limited impact, even though it was statistically significant ($P = 0.002$), on survival in GBM108-Vector tumors with a 7.5 day increase in median survival prolongation when compared to placebo (Fig. 4C). In contrast, SAR405838 treatment was markedly more effective in GBM108-VEGFA tumors with a 45day prolongation in median survival as compared with placebo treatment ($P < 0.0001$; Fig. 4D). This observed increase in efficacy in the VEGFA-secreting tumors was even more remarkable in light of the fact that the VEGFA tumors had a more aggressive growth pattern (the median survival of GBM108-VEGFA placebo group and GBM108-Vector placebo group were 32 and 45 days, respectively), undoubtedly due to the stimulation of angiogenesis in the tumor (27, 28). The treatment effect was significantly greater in GBM108-VEFGA than in GBM108-Vector ($P < 0.0001$ by log rank and Wilcoxon test). Although differences in the microenvironment associated with VEGFA expression cannot be completely discounted, these data strongly suggest that limited drug distribution across a

relatively intact BBB in the parental GBM108 PFX model critically limits the efficacy of SAR405838.

Discussion

The vital role of MDM2 in regulating p53 function makes MDM2 inhibitors an attractive drug class for further exploration and clinical development. MDM2 inhibitors demonstrate efficacy in a variety of cell types and at least seven novel agents are currently undergoing phase I investigation for several solid tumors (29–31). This study joins a growing body of literature suggesting that MDM2 inhibition also represents a promising therapeutic strategy for a sub-population of GBM (32–34). Here, we demonstrate that the MDM2 inhibitor SAR405838 can induce the expression of downstream p53 targets PUMA and p21 in p53 wild-type/MDM2 over-expressed GBM lines. SAR405838 treatment results in increased apoptosis and a reduction in neurosphere formation in sensitive lines. *In vivo* flank experiments demonstrate both increased apoptosis and profound suppression of tumor volume with SAR405838 treatment in a sensitive line (GBM108), suggesting a cytotoxic mechanism. However, little efficacy was seen in a p53 wild-type line without MDM2 over-expression (GBM102). In conjunction with a recent study in GBM evaluating another MDM2 inhibitor (RG7112), the current study confirms significant resistance to MDM2 inhibition associated

Figure 4.
Improved pharmacodynamic response and orthotopic survival in GBM108-VEGFA. **A,** p21 expression in GBM108-Vector and GBM108-VEGFA after SAR405838 treatment in orthotopic tumors (scale bar, 200 μm). **B,** Quantitation of SAR405838 effect on p53 signaling. Mice with established orthotopic tumors were treated with SAR405838 or placebo and then processed for p21 IHC. The percentage of p21-positive nuclei per high powered field in GBM108-Vector versus GBM108-VEGFA after placebo or SAR405838 (5 mice/group) are presented as mean ± standard deviation. **C** and **D,** Orthotopic survival, GBM108-Vector ($n = 10$ per group) versus GBM108-VEGFA ($n = 9$ for placebo and $n = 10$ for the treatment group). SAR405838 was dosed at 50 mg/kg p.o. qd until moribund.

with TP53 mutation and robust sensitivity associated with MDM2 amplification (34).

This study also highlights the critical role of drug delivery in the successful application of targeted therapy for GBM. We demonstrate that MDM2 inhibition can have profound efficacy in appropriately selected GBM, but limited drug delivery across the BBB may severely restrict the intracranial efficacy of SAR405838. Disruption of the BBB through VEGFA overexpression results in both markedly increased intratumoral accumulation of SAR405838 and increased p21 expression when compared with the empty vector control. Mice with BBB-disrupted tumors also experienced a survival benefit with SAR405838 treatment whereas mice with mostly BBB-intact tumors derived no benefit from treatment. Considering the fact that G108-VEGFA tumors are intrinsically more virulent compared to G108-Vector due to the effect of VEGFA expression on angiogenesis and hence on glioblastoma growth, the survival benefit that we have seen here is even more pronounced with SAR405838 treatment (27, 28). These data suggest that small-molecule MDM2 inhibitors may have profound efficacy in appropriately selected patients only if a sufficiently brain-penetrant agent can be identified. Similar correlations with limited brain penetration for otherwise highly

effective drugs suggest that this may be a generalizable phenomenon (35–40).

Interestingly, relatively BBB-intact tumors in our study maintained visible levels of contrast enhancement on T1-weighted MR imaging despite the lack of significant drug accumulation on MALDI MSI. Though contrast enhancement does indicate a certain degree of BBB disruption, patient biopsy studies of contrast enhancing brain regions following repeated MR scans demonstrate that elemental concentrations of gadolinium as low as 0.3 μg/mg (1.9 nmol/L) are sufficient to generate T1 signal changes (41–45). Making the assumption that targeted agents have similar CNS distribution characteristics as gadolinium, such low concentrations are often below the threshold required for clinical activity. This work seriously calls into question the likely misguided notion that contrast enhancement as seen on clinical imaging equates with pharmacologically meaningful drug accumulation of brain impenetrant agents, such as SAR405838, in GBM (46). Even in regions of contrast enhancement, drug delivery into GBM may be limited by a heterogeneously intact BBB, significantly limiting the efficacy of drug treatment.

Issues with brain-penetration for targeted therapies also extend to therapy for brain metastases. Individualized medicine

approaches based upon targeted therapies have improved systemic disease control in appropriately selected cancer types including melanomas with BRAF V600E mutations, non–small cell lung cancer (NSCLC) with EML4–ALK fusions, and colon cancer with wild-type KRAS. Despite these successes in controlling peripheral disease, CNS metastases remain a substantial problem. Upwards to 60% of NSCLC patients develop CNS metastases while on crizotinib treatment, whereas treatment with trastuzumab in HER2$^+$ breast cancer is associated with a 35% increase in relative risk of CNS metastases (47, 48). The likely cause of such isolated CNS failure is poor penetration of the BBB by these targeted agents (49). As peripheral disease control improves with new therapies, strategies for decreasing CNS disease burden may become the primary driver for overall survival.

Thus far, no phase III clinical trials using targeted agents in GBM have resulted in improved overall survival. Given that many of these agents have limited BBB permeability (50), our results suggest that selection of a drug with optimal brain distribution is a critical consideration in designing and implementing future trials using targeted agents in the context of precision medicine strategies for GBM.

Disclosure of Potential Conflicts of Interest

I. Meaux, C. Barriere, L. Debussche, and J. Watters are employees of Sanofi who also own stock in the company. N. Agar is a co-founder of BayesianDx and a scientific advisor to inviCRO. No potential conflicts of interest were disclosed by the other authors.

Authors' Contributions

Conception and design: M. Kim, D.J. Ma, S. Zhang, K.E. Parrish, C Barriere, L. Debussche, J. Watters, I.F. Parney, N.Y.R. Agar, W.F. Elmquist, J.N. Sarkaria

Development of methodology: M. Kim, D.J. Ma, D. Calligaris, S. Zhang, I. Meaux, F. Jin, G.J. Kitange, A.J. Johnson, J.N. Sarkaria

Acquisition of data (provided animals, acquired and managed patients, provided facilities, etc.): M. Kim, D.J. Ma, D. Calligaris, S. Zhang, R.W. Feathers, I. Meaux, A.C. Mladek, K.E. Parrish, A.J. Johnson, I.F. Parney, N.Y.R Agar

Analysis and interpretation of data (e.g., statistical analysis, biostatistics, computational analysis): M. Kim, D.J. Ma, D. Calligaris, R.W. Feathers, R.A. Vaubel, I. Meaux, A.C. Mladek, C Barriere, S. Tian, P.A Decker, J.E. Eckel-Passow, I.F. Parney, P.Z. Anastasiadis, N.Y.R. Agar, W.F. Elmquist, J.N. Sarkaria

Writing, review, and/or revision of the manuscript: M. Kim, D.J. Ma, D. Calligaris, I. Meaux, K.E. Parrish, L. Debussche, P.A Decker, J.E. Eckel-Passow, G.J. Kitange, A.J. Johnson, I.F. Parney, P.Z. Anastasiadis, N.Y.R. Agar, W.F. Elmquist, J.N. Sarkaria

Study supervision: P.Z. Anastasiadis, W.F. Elmquist, J.N. Sarkaria

References

1. Vitucci M, Hayes DN, Miller CR. Gene expression profiling of gliomas: merging genomic and histopathological classification for personalised therapy. Br J Cancer 2011;104:545–53.
2. Deeken JF, Loscher W. The blood-brain barrier and cancer: transporters, treatment, and Trojan horses. Clin Cancer Res 2007;13:1663–74.
3. Doolittle ND, Peereboom DM, Christoforidis GA, Hall WA, Palmieri D, Brock PR, et al. Delivery of chemotherapy and antibodies across the blood-brain barrier and the role of chemoprotection, in primary and metastatic brain tumors: report of the eleventh annual blood-brain barrier consortium meeting. J Neurooncol 2007;81:81–91.
4. Gerstner ER, Fine RL. Increased permeability of the blood-brain barrier to chemotherapy in metastatic brain tumors: establishing a treatment paradigm. J Clin Oncol 2007;25:2306–12.
5. Agarwal S, Sane R, Ohlfest JR, Elmquist WF. The role of the breast cancer resistance protein (ABCG2) in the distribution of sorafenib to the brain. J Pharmacol Exp Ther 2011;336:223–33.
6. Parrish KE, Sarkaria JN, Elmquist WF. Improving drug delivery to primary and metastatic brain tumors: strategies to overcome the blood-brain barrier. Clin Pharmacol Ther 2015;97:336–46.
7. Iqbal U, Abulrob A, Stanimirovic DB. Integrated platform for brain imaging and drug delivery across the blood-brain barrier. Methods Mol Biol 2011;686:465–81.
8. Pafundi DH, Laack NN, Youland RS, Parney IF, Lowe VJ, Giannini C, et al. Biopsy validation of 18F-DOPA PET and biodistribution in gliomas for neurosurgical planning and radiotherapy target delineation: results of a prospective pilot study. Neuro Oncol 2013;15:1058–67.
9. Comprehensive genomic characterization defines human glioblastoma genes and core pathways. Nature 2008;455:1061–8.
10. Wade M, Li YC, Wahl GM. MDM2, MDMX and p53 in oncogenesis and cancer therapy. Nat Rev Cancer 2013;13:83–96.
11. Hu B, Gilkes DM, Chen J. Efficient p53 activation and apoptosis by simultaneous disruption of binding to MDM2 and MDMX. Cancer Res 2007;67:8810–7.
12. Liu M, Li C, Pazgier M, Mao Y, Lv Y, Gu B, et al. D-peptide inhibitors of the p53-MDM2 interaction for targeted molecular therapy of malignant neoplasms. Proc Natl Acad Sci U S A 2010;107:14321–6.
13. Villalonga-Planells R, Coll-Mulet L, Martinez-Soler F, Castano E, Acebes JJ, Gimenez-Bonafe P, et al. Activation of p53 by nutlin-3a induces apoptosis and cellular senescence in human glioblastoma multiforme. PLoS ONE 2011;6:e18588.
14. Wang S, Sun W, Zhao Y, McEachern D, Meaux I, Barriere C, et al. SAR405838: an optimized inhibitor of MDM2-p53 interaction that induces complete and durable tumor regression. Cancer Res 2014;74:5855–65.
15. Kitange GJ, Mladek AC, Carlson BL, Schroeder MA, Pokorny JL, Cen L, et al. Inhibition of histone deacetylation potentiates the evolution of acquired temozolomide resistance linked to MGMT upregulation in glioblastoma xenografts. Clin Cancer Res 2012;18:4070–9.
16. Nadkarni A, Shrivastav M, Mladek AC, Schwingler PM, Grogan PT, Chen J, et al. ATM inhibitor KU-55933 increases the TMZ responsiveness of only inherently TMZ sensitive GBM cells. J Neurooncol 2012;110:349–57.
17. Maddika S, Kavela S, Rani N, Palicharla VR, Pokorny JL, Sarkaria JN, et al. WWP2 is an E3 ubiquitin ligase for PTEN. Nat Cell Biol 2011;13:728–33.
18. Gupta SK, Mladek AC, Carlson BL, Boakye-Agyeman F, Bakken KK, Kizilbash SH, et al. Discordant *in vitro* and *in vivo* chemopotentiating effects of the PARP inhibitor veliparib in temozolomide-sensitive versus-resistant glioblastoma multiforme xenografts. Clin Cancer Res 2014;20:3730–41.
19. Cen L, Carlson BL, Schroeder MA, Ostrem JL, Kitange GJ, Mladek AC, et al. p16-Cdk4-Rb axis controls sensitivity to a cyclin-dependent kinase inhibitor PD0332991 in glioblastoma xenograft cells. Neuro Oncol 2012;14:870–81.

20. Renner DN, Jin F, Litterman AJ, Balgeman AJ, Hanson LM, Gamez JD, et al. Effective treatment of established GL261 murine gliomas through picornavirus vaccination-enhanced tumor antigen-specific CD8+ T Cell Responses. PLoS ONE 2015;10:e0125565.

21. Renner DN, Malo CS, Jin F, Parney IF, Pavelko KD, Johnson AJ. Improved treatment efficacy of antiangiogenic therapy when combined with picornavirus vaccination in the GL261 glioma model. Neurotherapeutics 2016;13:226–36.

22. Liu X, Ide JL, Norton I, Marchionni MA, Ebling MC, Wang LY, et al. Molecular imaging of drug transit through the blood-brain barrier with MALDI mass spectrometry imaging. Sci Rep 2013;3:2859.

23. Hoffman-Luca CG, Yang CY, Lu J, Ziazadeh D, McEachern D, Debussche L, et al. Significant differences in the development of acquired resistance to the MDM2 inhibitor SAR405838 between in vitro and in vivo drug treatment. PLoS ONE 2015;10:e0128807.

24. Dobrogowska DH, Lossinsky AS, Tarnawski M, Vorbrodt AW. Increased blood-brain barrier permeability and endothelial abnormalities induced by vascular endothelial growth factor. J Neurocytol 1998;27:163–73.

25. Proescholdt MA, Heiss JD, Walbridge S, Muhlhauser J, Capogrossi MC, Oldfield EH, et al. Vascular endothelial growth factor (VEGF) modulates vascular permeability and inflammation in rat brain. J Neuropathol Exp Neurol 1999;58:613–27.

26. Argaw AT, Asp L, Zhang J, Navrazhina K, Pham T, Mariani JN, et al. Astrocyte-derived VEGF-A drives blood-brain barrier disruption in CNS inflammatory disease. J Clin Invest 2012;122:2454–68.

27. Weathers SP, de Groot J. VEGF manipulation in glioblastoma. Oncology 2015;29:720–7.

28. Claffey KP, Robinson GS. Regulation of VEGF/VPF expression in tumor cells: consequences for tumor growth and metastasis. Cancer Metastasis Rev 1996;15:165–76.

29. Bill KL, Garnett J, Meaux I, Ma X, Creighton CJ, Bolshakov S, et al. SAR405838: a novel and potent inhibitor of the MDM2:p53 axis for the treatment of dedifferentiated liposarcoma. Clin Cancer Res 2016;22: 1150–60.

30. Hai J, Sakashita S, Allo G, Ludkovski O, Ng C, Shepherd FA, et al. Inhibiting MDM2-p53 interaction suppresses tumor growth in patient-derived non-small cell lung cancer xenograft models. J Thorac Oncol 2015;10:1172–80.

31. Deben C, Wouters A, Op de Beeck K, van Den Bossche J, Jacobs J, Zwaenepoel K, et al. The MDM2-inhibitor Nutlin-3 synergizes with cisplatin to induce p53 dependent tumor cell apoptosis in non-small cell lung cancer. Oncotarget 2015;6:22666–79.

32. Chen X, Tai L, Gao J, Qian J, Zhang M, Li B, et al. A stapled peptide antagonist of MDM2 carried by polymeric micelles sensitizes glioblastoma to temozolomide treatment through p53 activation. J Control Release 2015;218:29–35.

33. Daniele S, Barresi E, Zappelli E, Marinelli L, Novellino E, Da Settimo F, et al. Long lasting MDM2/Translocator protein modulator: a new strategy for irreversible apoptosis of human glioblastoma cells. Oncotarget 2016;7: 7866–84.

34. Verreault M, Schmitt C, Goldwirt L, Pelton K, Haidar S, Levasseur C, et al. Preclinical efficacy of the MDM2 inhibitor RG7112 in MDM2-amplified and TP53 wild-type glioblastomas. Clin Cancer Res 2016;22:1185–96.

35. Vaidhyanathan S, Mittapalli RK, Sarkaria JN, Elmquist WF. Factors influencing the CNS distribution of a novel MEK-1/2 inhibitor: implications for combination therapy for melanoma brain metastases. Drug Metab Dispos 2014;42:1292–300.

36. Becker CM, Oberoi RK, McFarren SJ, Muldoon DM, Pafundi DH, Pokorny JL, et al. Decreased affinity for efflux transporters increases brain penetrance and molecular targeting of a PI3K/mTOR inhibitor in a mouse model of glioblastoma. Neuro Oncol 2015;17:1210–9.

37. Parrish KE, Cen L, Murray J, Calligaris D, Kizilbash S, Mittapalli RK, et al. Efficacy of PARP inhibitor rucaparib in orthotopic glioblastoma xenografts is limited by ineffective drug penetration into the central nervous system. Mol Cancer Ther 2015;14:2735–43.

38. Parrish KE, Pokorny J, Mittapalli RK, Bakken K, Sarkaria JN, Elmquist WF. Efflux transporters at the blood-brain barrier limit delivery and efficacy of cyclin-dependent kinase 4/6 inhibitor palbociclib (PD-0332991) in an orthotopic brain tumor model. J Pharmacol Exp Ther 2015;355:264–71.

39. Pokorny JL, Calligaris D, Gupta SK, Iyekegbe DO Jr., Mueller D, Bakken KK, et al. The efficacy of the wee1 inhibitor MK-1775 combined with temozolomide is limited by heterogeneous distribution across the blood-brain barrier in glioblastoma. Clin Cancer Res 2015;21:1916–24.

40. Zhang C, Liu J, Tan C, Yue X, Zhao Y, Peng J, et al. microRNA-1827 represses MDM2 to positively regulate tumor suppressor p53 and suppress tumorigenesis. Oncotarget 2016;7:8783–96.

41. McDonald RJ, McDonald JS, Kallmes DF, Jentoft ME, Murray DL, Thielen KR, et al. Intracranial gadolinium deposition after contrast-enhanced MR imaging. Radiology 2015;275:772–82.

42. Radbruch A, Weberling LD, Kieslich PJ, Eidel O, Burth S, Kickingereder P, et al. Gadolinium retention in the dentate nucleus and globus pallidus is dependent on the class of contrast agent. Radiology 2015;275:783–91.

43. Ramalho J, Castillo M, AlObaidy M, Nunes RH, Ramalho M, Dale BM, et al. High signal intensity in globus pallidus and dentate nucleus on unenhanced T1-weighted MR images: evaluation of two linear gadolinium-based contrast agents. Radiology 2015;276:836–44.

44. Robert P, Lehericy S, Grand S, Violas X, Fretellier N, Idee JM, et al. T1-weighted hypersignal in the deep cerebellar nuclei after repeated administrations of gadolinium-based contrast agents in healthy rats: difference between linear and macrocyclic agents. Invest Radiol 2015;50:473–80.

45. Weberling LD, Kieslich PJ, Kickingereder P, Wick W, Bendszus M, Schlemmer HP, et al. Increased signal intensity in the dentate nucleus on unenhanced T1-weighted images after gadobenate dimeglumine administration. Invest Radiol 2015;50:743–8.

46. Boult JK, Borri M, Jury A, Popov S, Box G, Perryman L, et al. Investigating intracranial tumour growth patterns with multiparametric MRI incorporating Gd-DTPA and USPIO-enhanced imaging. NMR Biomed 2016;29: 1608–17.

47. Olson EM, Abdel-Rasoul M, Maly J, Wu CS, Lin NU, Shapiro CL. Incidence and risk of central nervous system metastases as site of first recurrence in patients with HER2-positive breast cancer treated with adjuvant trastuzumab. Ann Oncol 2013;24:1526–33.

48. Rangachari D, Yamaguchi N, VanderLaan PA, Folch E, Mahadevan A, Floyd SR, et al. Brain metastases in patients with EGFR-mutated or ALK-rearranged non-small-cell lung cancers. Lung Cancer 2015;88:108–11.

49. Shi W, Dicker AP. CNS metastases in patients with non-small-cell lung cancer and ALK gene rearrangement. J Clin Oncol 2016;34:107–9.

50. Agarwal S, Sane R, Oberoi R, Ohlfest JR, Elmquist WF. Delivery of molecularly targeted therapy to malignant glioma, a disease of the whole brain. Expert Rev Mol Med 2011;13:e17.

Molecular Cancer Therapeutics

Efficacy of the MDM2 Inhibitor SAR405838 in Glioblastoma Is Limited by Poor Distribution Across the Blood−Brain Barrier

Minjee Kim, Daniel J. Ma, David Calligaris, et al.

Updated version	Access the most recent version of this article at: doi:10.1158/1535-7163.MCT-17-0600
Supplementary Material	Access the most recent supplemental material at: http://mct.aacrjournals.org/content/suppl/2018/07/03/1535-7163.MCT-17-0600.DC1

Cited articles	This article cites 50 articles, 15 of which you can access for free at: http://mct.aacrjournals.org/content/17/9/1893.full#ref-list-1
Citing articles	This article has been cited by 1 HighWire-hosted articles. Access the articles at: http://mct.aacrjournals.org/content/17/9/1893.full#related-urls

E-mail alerts	Sign up to receive free email-alerts related to this article or journal.
Reprints and Subscriptions	To order reprints of this article or to subscribe to the journal, contact the AACR Publications Department at pubs@aacr.org.
Permissions	To request permission to re-use all or part of this article, use this link http://mct.aacrjournals.org/content/17/9/1893. Click on "Request Permissions" which will take you to the Copyright Clearance Center's (CCC) Rightslink site.